Structure, Energetics, and Reactivity of Boric Acid Nanotubes: A Molecular Tailoring Approach

M. Elango,[†] V. Subramanian,[*,†] Anuja P. Rahalkar,[‡] Shridhar R. Gadre,[*,‡] and N. Sathyamurthy[*,§,||]

Chemical Laboratory, Central Leather Research Institute, Council of Scientific and Industrial Research, Adyar, Chennai, India 600 020, Department of Chemistry, University of Pune, Pune, India 411 007, and Indian Institute of Science Education and Research (IISER) Mohali, Chandigarh, India 160 019

Received: March 29, 2008

Cardinality guided molecular tailoring approach (CG-MTA) [Ganesh et al. *J. Chem. Phys.* **2006**, *125*, 104019] has been effectively employed to perform ab initio calculations for large molecular clusters of boric acid. It is evident from the results that boric acid forms nanotubes, structurally similar to carbon nanotubes, with the help of an extensive hydrogen-bonding (H-bonding) network. Planar rosette-shaped hexamer of boric acid is the smallest repeating unit in such nanotubes. The stability of these tubes increases due to enhancement in the number of H-bonding interactions as the diameter increases. An analysis of molecular electrostatic potential (MESP) of these systems provides interesting features regarding the reactivity of these tubes. It is predicted that due to alternate negative and positive potentials on O and B atoms, respectively, boric acid nanotubes will interact favorably with polar systems such as water and can also form multiwalled tubes.

Introduction

The discovery of fullerene and carbon nanotube is responsible for the intensive activity in various branches of science to design and develop new materials at the nano scale and their applications.[1,2] Nanomaterials exhibit mechanical, electronic, and optical properties that are different from those at the bulk level. In the design of these materials, the chemical bonding in elemental carbon plays a crucial role. Each carbon atom bonds invariably with three carbon atoms to form a variety of balls and tubes. Along these lines, several nanomaterials based on BN, SiO_2, MoS_2, V_2O_5, and ZnO have been synthesized.

Nature has wonderful examples for nanomaterials in biology.[3] There are numerous proteins and nucleic acids having dimensions of the order of 10^{-9} m.[3] These molecules are stabilized by hydrogen bonding, in addition to other interactions.[3b,c] The strength of H-bonding interaction lies between weak van der Waals interaction and strong covalent bonding.[4] Because of its geometrical characteristics, H-bond helps in forming a variety of supramolecular aggregates at various levels.[5] The importance of H-bonding in the supramolecular chemistry has received widespread attention. It is evident from earlier studies[6] that there is enough scope for designing new nanomaterials with H-bonding by appropriate selection of basic building blocks.

In this context, orthoboric acid (boric acid) is an interesting example. The crystal structure of boric acid[7] has structural features that are similar to those of graphite and MoS_2. In each boric acid layer, one boron atom is surrounded by three oxygen atoms to form triangular BO_3 groups, which form H-bonds with other planar BO_3 groups. As a result, boric acid serves as a good building block for supramolecular H-bonded structures, with the help of the three −OH groups oriented in a planar triangular geometry. It is expected that a variety of hydrogen-bonded assemblies can be formed by intermolecular interaction of orthoboric acid. This is vindicated by the recent experimental work by Li et al.[8] They have reported the synthesis and growth of orthoboric acid nano- and microscale structures. Depending on the relative humidity, temperature, and exposure time to humid atmosphere, it is possible to design nanotubes, nanotips, nanorods, microtubes, or microtips. These novel structures could have potential applications in submicrometer-scale devices and sensors. Their unique properties, such as self-lubrication and dehydration in a vacuum, may have promising application in tribology. Boric acid is also used in various fields as an antiseptic agent, insecticide, flame retardant, and food preservative. It is thus expected that the nanomaterials designed from boric acid may have commercial application in these fields.

With a view to understand the structure and stability of boric acid nanostructures, Hartree−Fock (HF) and Density Functional Theory (DFT) calculations have been performed to investigate the family of cage-shaped boric acid clusters.[9] Zigzag and armchair nanotubes of ortho- and metaboric acid clusters have been studied using the density functional theory-based discrete variation (DFT-DV) method by Enyashin et al.[10] They have found that fabrication of boric acid nanotubes requires much less energy than the synthesis of most popular carbon nanotubes. In addition to this, they have found that orthoboric acid aggregates more preferably in tubular form than does metaboric acid. Ab initio quantum chemical calculations suggest that boric acid molecules can self-assemble into bowls and balls.[11] The role of cyclic pentamer and cyclic hexamer in deciding the formation of nonplanar bowls and planar sheets has been pointed out. The origin of boric acid ball structure has also been traced. These calculations have clearly brought out the usefulness of computational chemistry methods in the de novo design of nanomaterials.

* Corresponding authors. Phone: +91 44 24411630 (V.S.), +91-20-2560-1228 (S.R.G.), +91-172-2790188 (N.S.). Fax: +91 44 24911589 (V.S.), +91-20-2569-1728 (S.R.G.), +91-172-2790188 (N.S.). E-mail: subuchem@hotmail.com (V.S.), gadre@chem.unipune.ernet.in (S.R.G.), nsath@iitk.ac.in (N.S.).

[†] Central Leather Research Institute.

[‡] University of Pune.

[§] IISER.

[||] Honorary Professor, Jawaharlal Nehru Centre for Advanced Scientific Research, Bangalore 560 064, India.

10.1021/jp802723e CCC: $40.75
Published on Web 07/25/2008

However, large clusters of boric acid containing several tens of monomer units have not yet been studied using ab initio methods. This is because of high scaling orders of ab initio methods. For a system with N basis functions, the complexity of the calculation varies typically as $O(N^3)$ for HF, $O(N^5)$ for Møller-Plessete second order perturbation theory (MP2), going up to $O(N^7)$ for correlated methods. Hence, for molecular systems with more than 100 atoms, huge computational resources and storage capacity are required. One way to overcome this high scaling problem is to use the divide-and-conquer (DC) type algorithm. One such linear scaling technique, the Cardinality Guided Molecular Tailoring Approach (CG-MTA), has been developed by Gadre and co-workers.[12–15] This method is applicable for one-electron property calculation, evaluation of single point energy and its derivatives, as well as for geometry optimization at ab initio level for large molecules and molecular clusters. This method has been coded into a locally modified version of a public domain ab initio package GAMESS.[16]

In the present study, an attempt has been made to design large boric acid clusters forming nanorings and nanotubes using CG-MTA. Such large molecular systems could not be studied easily using conventional methods. It is well-known that the stability of the carbon nanotube is related to its dimensions and mode of formation in which a sheet is rolled into a tube. As the diameter of the carbon nanotube increases, the stability of the nanotube increases.[17] Hence, it is necessary to understand the correlation between the stability of the boric acid-based nanotube and its geometrical parameters. For this, nanorings and nanotubes of boric acid formed in zigzag fashion, with the number of monomer units starting from 10 to 64 are optimized using CG-MTA, and the effect of various diameters on the formation of boric acid nanotubes has been investigated for the first time. In addition to the design of nanomaterials for understanding their reactivity, it is necessary to map out the molecular electrostatic potential. The CG-MTA has been used to plot the MESP map of these nanomaterials.

Methodology

A. Cardinality Guided Molecular Tailoring Approach. Cardinality Guided Molecular Tailoring Approach (CG-MTA) is a linear scaling technique developed for ab initio treatment of large molecular systems.[12–15] It is based on the divide-and-conquer (DC) type of algorithm in which the main problem is broken down to smaller subproblems, which are manageable. The methodology of CG-MTA can be briefly outlined as follows (for details, see refs 12–15):

(1) The supermolecule is fragmented into a set of smaller overlapping fragments.

(2) A cardinality expression is set up for the energy and its derivatives.

(3) Ab initio calculations are performed on the individual fragments at the appropriate level of theory.

(4) Energy and its derivatives with respect to nuclear coordinates are evaluated for the supermolecule, as per the cardinality expression given in eqs 1 and 2 (see below). These gradients are then utilized for driving the geometry optimization of the supermolecule.

The crux of CG-MTA is the fragmentation of the supermolecule and the cardinality expression. During the fragmentation, it is ensured that no multiple bonds or aromatic rings are cut.[12,13a] Dummy hydrogen atoms are added to satisfy the valencies wherever a covalent bond is cut. In the case of molecular clusters, the monomer units are kept intact, and only weak bonds such as H-bonds are scissored so that there is no need of addition of dummy atoms. The cardinality-based expressions given below for energy and its derivatives ensure that the contributions due to the dummy atoms are nullified.

For CG-MTA, cardinality refers to the number of atoms and bonds in a fragment. On the basis of set inclusion and exclusion principle, the cardinality expressions for energy and its derivatives are expressed as follows.[14a,15]

$$E = \sum E^{\mathrm{f}i} - \sum E^{\mathrm{f}i\cap \mathrm{f}j} + \cdots + (-1)^{k-1} \sum E^{\mathrm{f}i\cap \mathrm{f}j\cap \ldots \cap \mathrm{f}k} \tag{1}$$

$$\frac{\partial E}{\partial X_\mu} = \sum \frac{\partial E^{\mathrm{f}i}}{\partial X_\mu^{\mathrm{f}i}} - \sum \frac{\partial E^{\mathrm{f}i\cap \mathrm{f}j}}{\partial X_\mu^{\mathrm{f}i\cap \mathrm{f}j}} + \cdots + (-1)^{k-1} \sum \frac{\partial E^{\mathrm{f}i\cap \mathrm{f}j\cap \ldots \cap \mathrm{f}k}}{\partial X_\mu^{\mathrm{f}i\cap \mathrm{f}j\cap \ldots \cap \mathrm{f}k}} \tag{2}$$

where E denotes the estimate of the energy of the supermolecule, $E^{\mathrm{f}i}$ denotes the energy of fragment i, and $E^{\mathrm{f}i\cap \mathrm{f}j}$ denotes the energy of overlap of fragment i and fragment j. Similarly, eq 2 denotes the first derivatives of E, $E^{\mathrm{f}i}$, $E^{\mathrm{f}i\cap \mathrm{f}j}$ with respect to the nuclear coordinates, X_μ.

In particular, if there are two main fragments, f1 and f2, overlapping with each other, then the energy of the system is evaluated as:

$$E = E^{\mathrm{f}1} + E^{\mathrm{f}2} - E^{\mathrm{f}1\cap \mathrm{f}2} \tag{3}$$

Equation 1 is the generalization of this special case of two main fragments.

A parameter termed as *R*-goodness is defined for all of the atoms in the molecule as well as for the fragmentation scheme under consideration. This parameter provides a measure of how good the chemical environment of an atom is mimicked. Hence, the goodness of the scheme, which is the minimum of all of the atomic goodnesses, is an indicator of the reliability of the calculation. The higher is the *R*-goodness, the better is the accuracy. Benchmarking has shown that *R*-goodness of a fragmentation scheme between 3−4 Å is enough to produce sufficiently faithful results. Like *R*-goodness, there are various other parameters such as average size, scaling factor, etc., defined for a fragmentation scheme, which decide the quality of the fragments and in turn decide the accuracy and the computational cost of the calculation.

CG-MTA has been successfully applied for the calculation of one-electron properties, single point energy and gradient evaluations, as well as geometry optimization at HF and post-HF levels. Its benchmarking has been done using various structurally diverse nonlinear molecules. It is evident from the benchmarking results that CG-MTA not only speeds up these expensive calculations with minimal computational efforts but also produces sufficiently accurate results.

B. Computational Details. In the present work, various nanorings and nanotubes formed in zigzag fashion by orthoboric acid (BA) monomer units are studied. Nanorings chosen for this study consist of 10, 12, and 16 monomer units. Nanotubes open at both ends are formed by extensions of these nanorings. In addition to these structures, a test tube-shaped structure closed at one end formed by attaching a bowl shaped pentamer is also investigated in this work. All of these structures are optimized using CG-MTA method as described above. While fragmenting these structures, the option of keeping the monomer units intact is used; that is, covalent bonds within a monomer are not broken,

and hence no dummy atoms are added. Initially these structures are optimized at HF/6-31G level, followed by a final optimization at HF/6-31++G (d,p) level of theory, using CG-MTA enabled GAMESS, without any geometrical constraints. Although the HF method is extensively used for all of the calculations reported in this Article, to demonstrate the real power of CG-MTA, a few test runs are carried out at post-HF levels of theory such as DFT and MP2, for a nanotube made up of 40 boric acid monomers (**T40**). In one of these test runs, a few cycles of geometry optimization are run conventionally as well as using CG-MTA at B3LYP/3-21G, and their results are compared to ensure the accuracy of CG-MTA. Once CG-MTA is validated with this test run at DFT, complete CG-MTA-based geometry optimization of **T40** is carried out at B3LYP/6-31+G (d,p) level of theory. Further, some cycles of CG-MTA-based geometry optimization at MP2/6-31+G (d,p) level are also reported in the following section. The purpose of these studies is to demonstrate the feasibility of studying such a large system at correlated levels of theory. During optimization, no explicit use of symmetry is made, although the clusters are highly symmetric. For all of these rings and tubes, fragmentation schemes with *R*-goodness of 3.5−4.0 Å are used for CG-MTA optimization to ensure reliability of the calculations. Using the geometries optimized at HF/6-31++G (d,p) level, stabilization energy (ΔE) for the cluster and the average H-bond energy $\bar{E}_H$ are defined as follows:

$$\Delta E = (E_{cluster}) - n(E_{monomer}) \quad (4)$$

$$\overline{E}_H = \Delta E/N_H \quad (5)$$

Here, N_H is the number of H-bonds in a given structure.

Cross sections of these rings and tubes are not perfectly circular. Hence, the diameter of the ring or tube under consideration is determined as follows. If there are *n* monomer units with the B-atom at the center, then alternate *n*/2 of the B-atoms are coplanar and form a circle. The diameter of this circle is taken as the diameter of the given ring or tube.

For molecular clusters, it is important to correct the energies for basis set superposition error (BSSE). However, due to the large size of the clusters studied, computational cost for BSSE correction is prohibitively large. Further, it is not expected to change the trends in the binding energy of the clusters. Therefore, the present work does not report BSSE corrected energies for the clusters studied.

To get some idea about the reactivity of the clusters, MESP calculation is performed on a tube formed from 40 monomer units on a 100 × 100 × 100 grid at HF/6-31++G (d,p) level. This calculation is performed using an improved version of the web-based one-electron property calculator, Webprop.[18]

Results and Discussion

The H-bonding interaction between two boric acid units is similar to that in carboxylic acid dimer. Hence, a boric acid monomer can, in total, form six hydrogen bonds with three other boric acid molecules. Thus, it is indeed possible to design structurally diverse clusters of boric acid with the help of a network of O−H···O type of interactions. There are two basic building blocks for designing such clusters, bowl-shaped cyclic pentamer and planar cyclic hexamer. The cyclic pentameric motif of boric acids is the deciding structure in the formation and stabilization of boric acid balls.[11] In contrast, rosette-shaped planar cyclic hexameric structure (as given in Figure 1) is found to be more stable than other open and branched structures. The crystal structure of boric acid is made up of layers of these

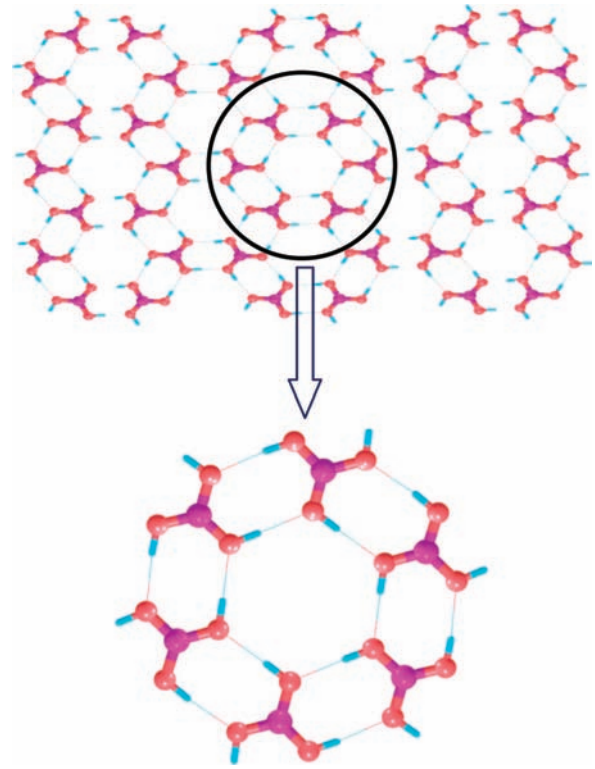

Figure 1. Rosette-shaped hexamer of ortho boric acid units. See text for details. Large pink spheres are boron atoms, large brown spheres are oxygen atoms, and small blue spheres are hydrogen atoms.

hydrogen-bonded networks of hexagon.[11] It is expected that this hexameric rosette plays a crucial role in the formation and the stabilization of boric acid-based nanotubes.

The structures of nanotubes $(BA)_n$ with n = 40, 45, 48, 64 (named as **T40**, **T45**, **T48**, **T64**, respectively), CG-MTA-optimized at HF/6-31++G (d,p) level, are shown in Figure 2. These elegantly formed structures reveal interesting symmetry and are stabilized due to the extensive hydrogen-bonding network.

The large sizes of the clusters and the corresponding number of basis set contractions involved in the calculations are noteworthy. The smallest among the clusters chosen for this study is **T40**, which consists of 280 atoms and 3760 contractions for 6-31++G (d,p) basis set, while the largest, **T64**, has 448 atoms and 6016 contractions for the same basis set (cf., Table 1). Because of a typical scaling of $O(N^3)$ for the HF method, geometry optimization of these clusters entails huge computational resources and therefore cannot be done routinely. However, the efficiency of the linear scaling CG-MTA method has made it possible to perform these geometry optimization calculations on a cluster of 8 Pentium IV @ 2.8 GHz with 2 GB RAM each. The typical time for completing one SCF cycle is 4−5 h on the above-mentioned hardware.

To validate the utility of CG-MTA for correlated level of theory, test runs are carried out at B3LYP/3-21G level involving 1680 contractions for **T40**. Each cycle of conventionally run geometry optimization at this level took about 7 h on a cluster of 4 Intel Core2Quad @ 2.4 GHz, each with 4 GB RAM and 250 GB hard disk. On the other hand, each cycle at the same level on the same hardware, when run with CG-MTA, took only about 2 h 20 min. Table 2 shows a comparison of actual and CG-MTA-based energy, gradients at each cycle of geometry optimization of **T40** at B3LYP/3-21G level.

There are 3640 contractions involved in geometry optimization of **T40** at B3LYP/6-31+G (d,p) and MP2/6-31+G (d,p)

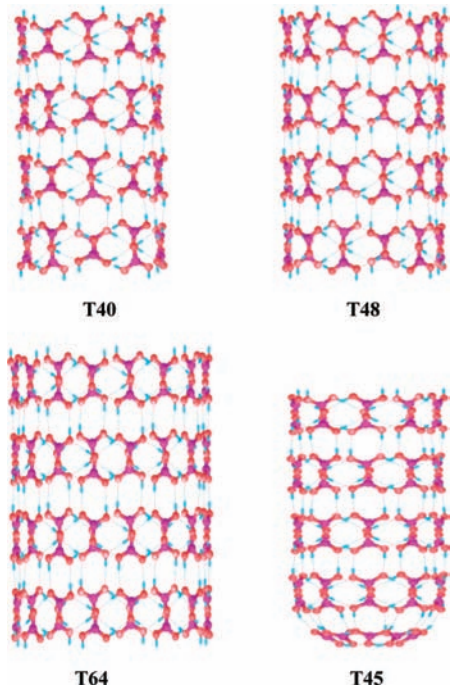

Figure 2. Views of nanotubes of boric acid units at different orientations, optimized at the HF/6-31++G (d,p) level of theory. See text for details.

TABLE 1: Stabilization Energy (ΔE) and Average H-bond Energy ($\bar{E}_H$) for Various Nanotubes of Boric Acid[a]

cluster name	no. of monomer units	tube diameter (Å)	N_H	ΔE (kcal/mol)	$\bar{E}_H$ (kcal/mol)
T40 (3760)	40	11.7	110	−508.19	−4.62
T48 (4512)	48	14.0	132	−619.43	−4.69
T64 (6016)	64	18.6	176	−842.40	−4.79
T45 (4230)	45	11.7	130	−591.56	−4.55

[a] Calculations were performed at HF/6-31++G (d,p) level. The number of contractions involved in the calculation is given in parentheses in the first column.

TABLE 2: Comparison of Actual and CG-MTA-Based Optimization of T40 at B3LYP/3-21G Level of Theory[a]

iteration	actual optimization	CG-MTA-based optimization
0	−10 041.59491	−10 041.59525
	0.0054	0.0049
	0.0017	0.0016
3	−10 041.59989	−10 041.59991
	0.0035	0.0034
	0.0007	0.0007
5	−10 041.60107	−10 041.60112
	0.0029	0.0025
	0.0005	0.0005

[a] For each iteration, the numbers given are energy, norm of maximum, and RMS gradients, respectively, in au.

levels, making it impossible to do these jobs conventionally with any given hardware that is available today. Yet such calculations are feasible using CG-MTA, which consumes a meager amount of time and computational power. Each cycle at B3LYP/6-31+G (d,p) level took about 2 h on a cluster of 12 Intel Core2Duo @ 2.8 GHz machines, each with 2 GB RAM and 80 GB hard disk, and at MP2/6-31+G (d,p) level took about 5 h 30 min on a cluster of 4 Intel Core2Quad @ 2.4 GHz machines, each with 4 GB RAM and 250 GB hard disk. This discussion emphasizes the time advantage due to CG-MTA and the ability of CG-MTA to run very huge calculations, while the accuracy of this method is discussed next.

Earlier benchmarks of CG-MTA have proved that a fragmentation scheme with minimum goodness between 3 to 4 Å produces energy estimates with errors within 1 millihartree, and the estimates of all numerically significant (with norm $>10^{-3}$) gradients are obtained to within 1−2% error. Keeping all this in mind, in all of the present calculations, a minimum goodness of ∼4.0 Å is maintained to ensure accuracy. To appraise the accuracy of the present calculations, a test of the results is done on **T40**. Two different fragmentation schemes for **T40**, one with a minimum goodness of 3.0 Å and the other with 4.1 Å, are used for single point energy evaluation for the final geometry obtained from the optimization. The energy estimates (in hartrees) of these schemes are −10 049.43254 and −10 049.43270, respectively. The difference is only ∼0.2 millihartree, indicating the consistency of the CG-MTA results for HF level calculations.

For correlated methods, tests for accuracy are carried out, and the results are given in Table 2, which confirm the reliability of CG-MTA at correlated methods. It is evident from Table 2, when actual and CG-MTA-based optimization runs are compared at B3LYP/3-21G level, the error in the CG-MTA energy estimate is less than 0.3 millihartree in each cycle. The largest error in the maximum gradient is 1.5×10^{-3}, other errors being of the order of 10^{-4}, while error in CG-MTA-based rms gradient is typically 1×10^{-4}. This is a representative example to show that CG-MTA is accurate enough for estimating energy and gradients even when correlated methods such as DFT and MP2 are used.

The calculated B−O bond length and B−O−H bond angle are 1.355 Å and 113.8°, respectively, for the monomer, which is in close agreement with the corresponding X-ray crystal structure[11] values of 1.361 Å and 114.0°. The calculated O−H bond length is 0.946 Å, while the calculated (O)H···O hydrogen- bond length in the dimer is 1.948 Å. The calculated (O)H···O hydrogen-bond length in the hexamer is 1.933 Å. The calculated (O)H···O hydrogen-bond lengths for the tubes range from 1.920 to 1.936 Å. These bond lengths and bond angles are calculated using geometries optimized at HF/6-31++G (d,p) level of theory.

The geometry of **T40** optimized at B3LYP/6-31+G (d,p) level shows B−O, O−H bond lengths of 1.374 and 0.980 Å, respectively, and B−O−H bond angle of 114.6°, with (O)H···O bond lengths ranging from 1.760 to 1.830 Å. Also, the overall structure of **T40** is seen to shrink slightly when optimized at B3LYP level, consequently decreasing the diameter of **T40** from 11.7 Å (for structure optimized at HF/6-31++G (d,p) level) to 11.3 Å.

Stabilization energies and average H-bond energies for the clusters evaluated using eqs 4 and 5 using CG-MTA energy estimates for the energy of the cluster are listed in Table 1. As the diameter of the nanotube increases, the stabilization energy also increases due to enhancement in the number of hydrogen-bonding interactions (cf., Table 1). As seen from Table 1, the stabilization energy per H-bond ranges from −4.55 to −4.79 kcal/mol. These values are comparable to those of water dimer and other classical hydrogen-bonded systems.[4d] The increase in the stabilization energy per H-bond for tubes of increasing diameter is only marginal. For **T40** optimized at B3LYP/6-31+G (d,p) level, the stabilization energy and average H-bond energy are −638.45 and −5.80 kcal/mol, respectively, which are numerically enhanced as compared to their HF-counterparts (cf., Table 1).

MESP is an important tool for investigating the reactivity of a molecular system. It gives an idea about the regions of electron localization in the molecule and therefore about the probable sites of electrophilic and nucleophilic attack. An earlier investigation was done[19] on fullerene (C_{60}), and it was found that all of the negative MESP values are on the outer side of the surface of C_{60} while the inner side is completely devoid of them. Similar MESP function calculation and topography analysis has been done for these nanotubes with a view to design hydrogen-bonded multiwalled tubes and also to assess their reactivity. Because the tubes **T48** and **T64** are structurally analogous to **T40**, MESP calculation is performed only on **T40**, at HF/6-31++G (d,p) level. Figure 3 depicts the top view of **T40** with MESP isosurfaces at −31.4, −18.8, and −12.6 kcal/mol. The minimum MESP value is found to be −37.7 kcal/mol. Starting from this minimum value and going in the direction of increasing MESP value, the isosurfaces are seen only at the terminal O-atoms at the edges of the tube. Topological analysis shows (3,+3) minima in this region are the deepest and have function values of −41.8 kcal/mol. This indicates that the terminal region of the tube is more reactive toward cations and other electropositive species. Further increasing the MESP value, at about −25.1 kcal/mol, isosurfaces start building on the outside surface of the tube. In this region, local (3,+3) minima are found to have values of −29.3 kcal/mol, indicating this surface as the next reactive region of the tube, where electrophiles can interact favorably. On further increment in MESP value, isosurfaces start appearing inside the tube at around −12.6 kcal/mol with (3,+3) minima at about −17.8 kcal/mol. Thus, negative potentials are present outside as well as inside the tube. Also, it is observed that there is no isosurface with a negative value around B-atoms, indicating the possibility of interaction with a nucleophile. Another view of this can be obtained from MESP textured on the van der Waals (vdW) surface of **T40** as depicted in Figure 4. The red and blue regions indicate negative and positive function values, respectively, colors fading to white as the function value approaches zero. Alternate red and blue regions on O and B atoms show that this is an ideal system for interaction with other polar systems such as water molecules.

As the two faces of the sheet of boric acid are equivalent, they will have identical MESP features such as alternate positive and negative potentials on the B and O atoms, respectively. It is evident from the MESP texturing on the vdW surfaces (cf., Figure 4. All the graphic depictions in this paper are done using MeTA Studio.[20]) for a tube that alternate positive and negative potentials are present outside as well as inside the tube, thereby implying that alternating MESP features of a sheet are retained when it is rolled into a tube. The crystal structure of boric acid reveals that it has stacked sheet structure akin to that of graphite and similar intermolecular interactions. Hence, from MESP studies, it can be predicted that if two stacked sheets are rolled giving rise to a multiwalled tube, then it could be stabilized in the same way as the two stacked sheets.

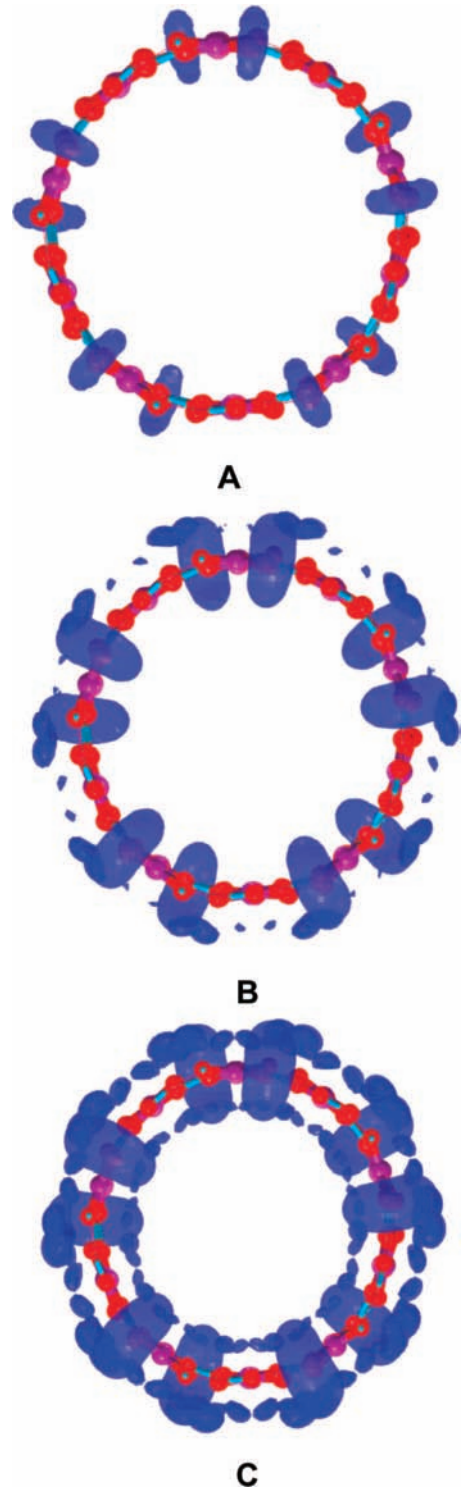

Figure 3. MESP isosurfaces for **T40** at −31.4 kcal/mol (A), −18.8 kcal/mol (B), and −12.6 kcal/mol (C). See text for details.

Summary and Conclusions

The current study clearly demonstrates the power of the cardinality guided molecular tailoring approach (CG-MTA) in performing ab initio calculations on large molecular clusters and predicting their structures and energetics. CG-MTA-based investigation suggests that boric acid molecules can self-assemble into a tubelike structure, similar to that of carbon nanotube. The planar cyclic hexamer structure (rosette) plays a key role in the formation of these tubes, and cyclic pentamer is vital in case of bowl-shaped curved surfaces (**T45**). It is worth pointing out that as the diameter of the boric acid nanotube increases, the number of H-bonding interactions and consequently the stabilization energy of the tube increases. It is interesting to note that the stabilization energy per H-bond in tubes with increasing diameters is nearly constant for all of the nanotubes investigated. This is due to (1) an increase in the number of hydrogen bonds and (2) lack of change in the geometrical parameters of each monomer as the diameter of the boric acid tube increases. Because the stabilization energy increases with diameter, it is possible to design tubes within tubes analogues of multiwalled carbon nanotubes. MESP

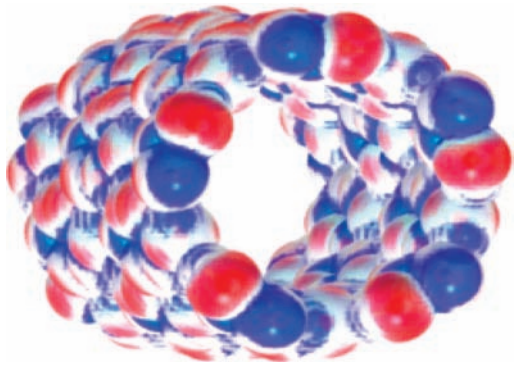

Figure 4. MESP textured on vdW surface of **T40**. See text for details.

analysis suggests favorable interaction of these nanotubes with polar molecular systems. MESP studies of the boric acid nanotube also support the feasibility of formation of multiwalled nanotubes. It should be emphasized here that such large clusters cannot be studied with the help of conventional electronic structure packages. Toward this end, linear scaling CG-MTA methodology offers an attractive tool to investigate such large clusters, their energetics and properties, without a significant loss of accuracy at HF and other higher correlated levels of theory.

Acknowledgment. We are thankful for the financial support from the Council of Scientific and Industrial Research (CSIR), New Delhi, India. Support from the UPE program of the University of Pune and the computational facility from the Center for Development of Advanced Computing (C-DAC), Pune, is gratefully acknowledged. S.R.G. and N.S. thank the Department of Science and Technology, New Delhi, for J. C. Bose Fellowships. M.E. and A.P.R. thank CSIR for Research Fellowships.

References and Notes

(1) Kroto, H. W.; Heath, J. R.; O'Brien, S. C.; Curl, R. F.; Smalley, R. E. *Nature* **1985**, *318*, 162.

(2) Iijima, S. *Nature* **1991**, *354*, 56.

(3) (a) Vo-Dinh, T. In *Protein Nanotechnology*; Vo-Dinh, T., Ed.; Human Press, 2005. (b) Saenger, W. *Principles of Nucleic Acid Structure*; Springer: New York, 1988. (c) Schulz, G. E.; Schirmer, R. H. *Principles of Protein Structure*; Springer: New York, 1996.

(4) (a) Steiner, T. *Angew. Chem., Int. Ed.* **2002**, *41*, 48. (b) Desiraju, G. R. *Acc. Chem. Res.* **2002**, *35*, 565. (c) Parthasarathi, R.; Subramanian, V. In *Hydrogen Bonding: New Insights*; Grabowski, S. J., Ed.; Challenges and Advances in Computational Chemistry and Physics 3; Kluwer: New York, 2006. (d) Parthasarathi, R.; Subramanian, V.; Sathyamurthy, N. *J. Phys. Chem. A* **2006**, *110*, 3349.

(5) (a) Jeffrey, G. A. *An Introduction to Hydrogen Bonding*; Oxford University Press:Oxford, NY, 1997. (b) Desiraju, G. R.; Steiner, T. *The Weak hydrogen bond in Structural Chemistry and Biology*; Oxford University Press: Oxford, 1999. (c) Scheiner, S. *Hydrogen Bonding. A Theoretical Perspective*; Oxford University Press: Oxford, 1997.

(6) (a) Lehn, J.-M. *Supramolecular Chemistry, Concepts and Perspectives*; VCH:Weinheim, 1995. (b) Steed, J. W.; Atwood, J. L. *Supramolecular Chemistry*; Wiley: Chichester, UK, 2000.

(7) Zachariasen, W. H. *Z. Kristallogr.* **1934**, *88*, 150. Zachariasen, W. H. Z. *Acta Crystallogr.* **1954**, *7*, 305.

(8) Li, Y.; Ruoff, R. S.; Chang, R. P. H. *Chem. Mater.* **2003**, *15*, 3276.

(9) (a) Wang, W.; Zhang, Y.; Huang, K. *J. Phys. Chem. B* **2005**, *109*, 8562. (b) Wang, W.; Zhang, Y.; Huang, K. *Chem. Phys. Lett.* **2005**, *405*, 425.

(10) Enyashin, A. N.; Ivanovskii, A. L. *Chem. Phys. Lett.* **2005**, *411*, 186.

(11) Elango, M.; Parthasarathi, R.; Subramanian, V.; Sathyamurthy, N. *J. Phys. Chem. A* **2005**, *109*, 8587.

(12) Gadre, S. R.; Shirsat, R. N.; Limaye, A. C. *J. Phys. Chem.* **1994**, *98*, 9165.

(13) (a) Babu, K.; Gadre, S. R. *J. Comput. Chem.* **2003**, *24*, 484. (b) Babu, K.; Ganesh, V.; Gadre, S. R.; Ghermani, N. E. *Theor. Chem. Acc.* **2004**, *111*, 255.

(14) (a) Ganesh, V.; Dongare, R. K.; Balanarayan, P.; Gadre, S. R. *J. Chem. Phys.* **2006**, *125*, 104019. (b) Ganesh, V.; Gadre, S. R. *J. Theor. Comput. Chem.* **2006**, *5*, 835.

(15) Gadre, S. R.; Rahalkar, A. P.; Ganesh, V. *IANCAS Bull.* **2006**, *4*, 267.

(16) Gordon, M.; et al. The GAMESS package, 2003.

(17) Saito, R.; Dresselhaus, G.; Dresselhaus, M. S. *Physical Properties of Carbon Nanotubes*; Imperial College Press: London, 1998.

(18) (a) Ganesh, V.; Kavatekar, R.; Rahalkar, A. P.; Gadre, S. R. J. Comput. Chem. **2008**, *29*, 488. (b) Bapat, S. V.; Shirsat, R. N.; Gadre, S. R. Chem. Phys. Lett. **1992**, *200*, 373. (c) Balanarayan, P.; Gadre, S. R. J. Chem. Phys. **2005**, *119*, 5037.

(19) Jemmis, E. D.; Subramanian, G.; Sastry, G. N.; Mehta, G.; Shirsat, R. N.; Gadre, S. R. *J. Chem. Soc., Perkin Trans.* **1996**, *2*, 2343.

(20) Ganesh, V. J. Comput. Chem. (in press) URL: http://code.google.com/p/metastudio/.

JP802723E